



1 **Changes in biomass burning, wetland extent, or agriculture**  
2 **drive atmospheric NH<sub>3</sub> trends in several African regions**

3

4

5

6 Jonathan E. Hickman<sup>1\*</sup>, Niels Andela<sup>2</sup>, Enrico Dammers<sup>3</sup>, Lieven Clarisse<sup>4</sup>, Pierre-François  
7 Coheur<sup>4</sup>, Martin Van Damme<sup>4</sup>, Courtney Di Vittorio<sup>5</sup>, Money Osohou<sup>6</sup>, Corinne Galy-  
8 Lacaux<sup>7</sup>, Kostas Tsigirdis<sup>1,8</sup>, Susanne Bauer<sup>1</sup>

9

10 <sup>1</sup>NASA Goddard Institute for Space Studies, New York, USA

11 <sup>2</sup>NASA Goddard Space Flight Center, Beltsville, USA

12 <sup>3</sup>Air Quality Research Division, Environment and Climate Change Canada, Toronto,  
13 Canada

14 <sup>4</sup>Université libre de Bruxelles (ULB), Service de Chimie Quantique et Photophysique,  
15 Atmospheric Spectroscopy, Brussels, Belgium

16 <sup>5</sup>Wake Forest University, Winston-Salem, USA

17 <sup>6</sup>Laboratoire de Physique de l'Atmosphère et de Mécanique des Fluides, Université  
18 Félix Houphouët-Boigny, Abidjan, Côte d'Ivoire

19 <sup>7</sup>Laboratoire d'Aérodynamique, Université Toulouse III Paul Sabatier / CNRS, France

20 <sup>8</sup>Columbia University, New York, USA

21

22 *\*Correspondence to: jonathan.e.hickman@nasa.gov*

23

24 **Abstract**

25 Atmospheric ammonia (NH<sub>3</sub>) is a precursor to fine particulate matter and a source  
26 of nitrogen (N) deposition that can adversely affect ecosystem health. The main sources of  
27 NH<sub>3</sub>—agriculture and biomass burning—are undergoing or expected to undergo  
28 substantial changes in Africa. Although evidence of increasing NH<sub>3</sub> over parts of Africa has



29 been observed, the mechanisms behind these trends are not well understood. Here we use  
30 observations of atmospheric  $\text{NH}_3$  vertical column densities (VCDs) from the Infrared  
31 Atmospheric Sounding Interferometer (IASI) along with other satellite observations of the  
32 land surface and atmosphere to evaluate how  $\text{NH}_3$  concentrations have changed over Africa  
33 from 2008 through 2017, and what has caused those changes. We find that  $\text{NH}_3$  VCDs have  
34 increased over several regions, including much of West Africa and parts of the Lake  
35 Victoria Basin. In West Africa  $\text{NH}_3$  VCDs are observed to increase during the late dry  
36 season, with increases of over  $6\% \text{ yr}^{-1}$  in Nigeria during February and March. These  
37 positive trends are associated with increasing burned area and CO trends during these  
38 months, likely related to agricultural preparation. Increases are also observed in the Lake  
39 Victoria Basin, where they are associated with expanding agricultural area. In contrast,  
40 South Sudan  $\text{NH}_3$  VCDs declined by over  $2\% \text{ yr}^{-1}$  during the February through May period,  
41 with the largest rates of change over the Sudd wetlands. Annual maxima in  $\text{NH}_3$  VCDs in  
42 South Sudan occur during February through May and are associated with drying of  
43 temporarily flooded wetland soils, which favor emissions of  $\text{NH}_3$ . The change in mean  $\text{NH}_3$   
44 VCDs over the Sudd and all of South Sudan during February through May is strongly  
45 correlated with variation in wetland extent in the Sudd: in years when more area remained  
46 flooded during the dry season,  $\text{NH}_3$  concentrations were higher ( $r=0.69$ ,  $p=0.03$ ).  
47 Relationships between agriculture and  $\text{NH}_3$  can be observed when evaluating national-  
48 scale statistics: countries with the largest declines in  $\text{NH}_3$  VCDs concentrations over time  
49 tended to have the smallest growth rates in crop productivity and livestock numbers as  
50 well as smaller negative changes in burned area than other countries. Fertilizer use in  
51 Africa is currently low but growing; implementing practices that can limit  $\text{NH}_3$  losses from  
52 fertilizer as agriculture is intensified may help mitigate impacts on health and ecosystems.

53

## 54 **1. Introduction:**

55

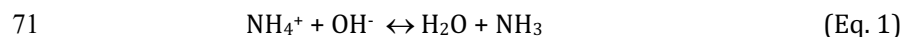
56 Ammonia ( $\text{NH}_3$ ), a reactive nitrogen (N) trace gas, plays a number of important roles  
57 in the atmosphere, with implications for human health, climate, and ecosystems. Once in  
58 the atmosphere,  $\text{NH}_3$  contributes to the production of inorganic aerosols, the primary  
59 constituents of fine particulate matter and a serious health hazard (Bauer et al., 2016;



60 Lelieveld et al., 2015; Pope et al., 2002). NH<sub>3</sub> can also be deposited to downwind  
61 ecosystems, contributing to eutrophication, soil acidification, vegetation damage,  
62 productivity declines, reductions in biodiversity, and indirect greenhouse gas emissions  
63 (Denier Van Der Gon and Bleeker, 2005; Krupa, 2003; Matson et al., 1999; Stevens et al.,  
64 2018; Tian and Niu, 2015).

65 Although NH<sub>3</sub> is emitted from natural soils, agriculture is by far the largest source of  
66 NH<sub>3</sub> globally (Behera et al., 2013; Bouwman et al., 1997). Urea fertilizer and livestock  
67 excreta are particularly important substrates for NH<sub>3</sub> formation, and can be volatilized  
68 quickly under favorable environmental conditions (Bouwman et al., 1997). In all soils, NH<sub>3</sub>  
69 is formed in solution following the dissociation of ammonium (NH<sub>4</sub><sup>+</sup>; Eq. 1).

70



72

73 Soil NH<sub>3</sub> production is temperature-dependent, doubling with every 5°C temperature  
74 increase, though the actual soil NH<sub>3</sub> flux is determined in part by plant and soil physiological  
75 and physical factors (Sutton et al., 2013). On average, fertilizer use has been extremely low  
76 in sub-Saharan Africa—often an order of magnitude or more lower than typical in Europe,  
77 the United States, or China (Hazell and Wood, 2008; Vitousek et al., 2009). Livestock manure  
78 N content also tends to be very low in sub-Saharan Africa (Rufino et al., 2006); the low  
79 manure quality and fertilizer use suggests that natural soils may be a more important source  
80 in the region than elsewhere in the world. However, agricultural intensification and  
81 increasing fertilizer use has been a central policy focus for many African countries, with  
82 national and regional efforts to increase N inputs by an order of magnitude or more (AGRA,  
83 2009).

84 After agriculture, biomass burning is the most important source of NH<sub>3</sub> globally  
85 (Bouwman et al., 1997), with roughly 60 to 70% of global NH<sub>3</sub> emissions from fires occurring  
86 in Africa (Cahoon et al., 1992; Whitburn et al., 2015). The amount of NH<sub>3</sub> emitted from  
87 biomass fires is controlled primarily by the type of burning that occurs. N in fuel is present  
88 predominantly in a chemically reduced state, and NH<sub>3</sub> is emitted in greater quantities from  
89 low temperature, smoldering combustion in which fuel N is incompletely oxidized (Goode et



90 al., 1999; Yokelson et al., 2008). Fuel moisture content, which can help determine whether  
91 combustion is smoldering or flaming, is thus an important determinant of biomass burning  
92  $\text{NH}_3$  emissions (Chen et al., 2010).

93 In contrast to other reactive N gases such as  $\text{NO}_x$  (nitric oxide + nitrogen dioxide),  
94  $\text{NH}_3$  emissions are typically unregulated outside of Europe (Anker et al., 2018; Kanter,  
95 2018; USDA Agricultural Air Quality Task Force, 2014), and substantial increasing trends  
96 have been observed by the NASA Atmospheric InfraRed Sounder (AIRS) over many of the  
97 world's major agricultural and biomass burning regions during the 21<sup>st</sup> century (Warner et  
98 al., 2017). West Africa has been identified as an important  $\text{NH}_3$  source region (Van Damme  
99 et al., 2018), where a trend of increasing  $\text{NH}_3$  concentrations over 2002 to 2013 has been  
100 attributed to increased fertilizer use (Warner et al., 2017). Increasing trends have also  
101 been observed over central Africa, and attributed to higher rates of biomass burning  
102 (Warner et al., 2017). However, the study by Warner et al. (2017) was global in nature,  
103 and as such could not include detailed explorations of the drivers of trends such as  
104 consideration of emission seasonality or the geographic distribution of emission drivers,  
105 which are particularly important across large parts of Africa where both biomass burning  
106 and soils are potentially important sources (van der A et al., 2008).

107 Here we use a ten-year satellite record to evaluate trends in atmospheric  $\text{NH}_3$   
108 concentrations over Africa from 2008 through 2017, including detailed examination of  
109 three regions where changes are pronounced: West Africa, the Lake Victoria Region, and  
110 South Sudan.

111

## 112 **2. Data and Methods**

### 113 **2.1 Global gridded data**

114 Multiple data products were used, including satellite observations and spatial  
115 datasets:

116 -The Infrared Atmospheric Sounding Interferometer (IASI-A), launched aboard the  
117 European Space Agency's MetOp-A in 2006, provides measurements of atmospheric  $\text{NH}_3$  and  
118 carbon monoxide (CO) twice a day (9:30 in the morning and evening, Local Solar Time at the  
119 equator). Here we use morning observations, when the thermal contrast is more favorable  
120 for retrievals (Clarisse et al., 2009; Van Damme et al., 2014a). The  $\text{NH}_3$  retrieval product



121 used (ANNI-NH<sub>3</sub>-v2.2R) follows a neural network retrieval approach. We refer to Van  
122 Damme et al. (2017) for a detailed description of the algorithm. For CO, we used the product  
123 obtained with the FORLI v20140922 retrieval algorithm (Hurtmans et al., 2012). Only  
124 observations with cloud cover below 20% were used. Given the absence of hourly or even  
125 daily observations of NH<sub>3</sub> concentrations in sub-Saharan Africa, the detection limit of IASI is  
126 difficult to determine with certainty. However, the region experiences high thermal contrast,  
127 and IASI seems to be able to reliably observe NH<sub>3</sub> down to 1 to 2 ppb at the surface (Clarisse  
128 et al., 2009; Van Damme et al., 2014b). We regridded the Level-2 IASI NH<sub>3</sub> and CO products  
129 to 0.25° × 0.25° resolution to match the resolution of other data used in the analysis. The  
130 IASI product has been validated using ground-based Fourier transform infrared (FTIR)  
131 observations of NH<sub>3</sub> total columns, with robust correlations at sites with high NH<sub>3</sub>  
132 concentrations, but lower at sites where atmospheric concentrations approach IASI's  
133 detection limits (Dammers et al., 2017). Compared to the FTIR observations, total columns  
134 from previous IASI NH<sub>3</sub> products (IASI-LUT and IASI-NNv1) are biased low by ~30% which  
135 varies per region depending on the local concentrations. IASI performed well in  
136 comparisons with surface observations of NH<sub>3</sub> concentrations in west and central Africa  
137 (Hickman et al., 2018; Ossohou et al., 2019). Validation of the IASI CO product using surface,  
138 aircraft, and satellite observations have found total columns to have an error that is generally  
139 below 10-15% in the tropics and mid-latitudes (George et al., 2009; Kerzenmacher et al.,  
140 2012; Pommier et al., 2010; De Wachter et al., 2012). The IASI NH<sub>3</sub> and CO products were  
141 used for the years 2008—the first full year of data available—to the end of 2017.

142 -The Tropical Rainfall Measuring Mission (TRMM) daily precipitation product (3B42)  
143 is based on a combination of TRMM observations, geo-synchronous infrared observations,  
144 and rain gauge observations (Huffman et al., 2007). Independent rain gauge observations  
145 from West Africa have been used to validate the product, with no indication of bias in the  
146 product (Nicholson et al., 2003).

147 - We used the NOAA Global Surface Temperature Dataset, a 0.5° gridded 2m monthly  
148 land surface temperature product (Fan and van den Dool, 2008). The data set is based on a  
149 combination of station observations from the Global Historical Climatology Network version



150 2 and the Climate Anomaly Monitoring System (GHCN\_CAMS), and uses an anomaly  
151 interpolation approach which relies on observation-based reanalysis data to derive spatio-  
152 temporal variation in temperature lapse rates for topographic temperature adjustment.

153 -We used the 500m MCD64A1 collection 6 Moderate Resolution Imaging  
154 Spectroradiometer (MODIS) burned area product for the period 2008-2017 (Giglio et al.,  
155 2018). The burned area data are aggregated by month and gridded to 0.25° resolution, and  
156 do not include burned area from small fires.

157 -We also used the MODIS MCD12C1 (collection 5) land cover product, which provides  
158 the percentage of cropped area in each 0.25° grid cell (Friedl et al., 2002). In Africa,  
159 agriculture is often practiced in complex mosaics of agricultural and natural land cover, so  
160 we used both the crop and crop/natural area mosaic MODIS classifications as agricultural  
161 area in our analysis.

162 -We used data on the spatio-temporal distribution of armed conflict events from the  
163 Armed Conflict Location & Event Data Project (ACLED; Raleigh et al., 2010). We included  
164 data for both violent and non-violent conflict events over the period 2008-2017.

## 165 **2.2 Sudd wetland extent**

166 Monthly flooded area extents of the Sudd Wetland from 2000 to 2018 were derived  
167 from 8-day composite MODIS land surface reflectance imagery (MOD09A1); data from 2005  
168 through 2017 were used in the analyses. We refer to Di Vittorio and Georgakakos (2018) for  
169 a detailed description of the classification procedure designed to retrieve these data. In  
170 summary, monthly flood maps were obtained through a two-stage classification procedure.  
171 The first stage used the full 18-year data set to produce a wetland land cover map that  
172 distinguishes between wetland vegetation classes and their flooding regimes (permanently  
173 flooded, seasonally flooded, or non-flooded). The second stage compares seasonally flooded  
174 pixels from each vegetation class to their non-flooded counterparts on a monthly basis to  
175 identify the timing and duration of flooding for each pixel. These data were originally derived  
176 to calibrate a hydrologic model of the Sudd that is dependent on Nile flows; therefore, a  
177 connectivity algorithm was applied to ensure that all flooded pixels were physically



178 connected to the Nile River. A few adjustments have been made to the previously published  
179 dataset for the application of this study. The classification algorithm has been improved to  
180 more accurately capture the inter-annual fluctuations in the permanently flooded areas. The  
181 dataset was also extended through the end of 2017, and the total flooded area was quantified  
182 prior to applying the connectivity algorithm. The magnitudes of the monthly flooded area  
183 estimates are now substantially larger because they include areas flooded from local runoff  
184 in addition to areas flooded by the Nile River.

185

### 186 **2.3 Spatial and national analyses**

187 We evaluated spatial relationships between mean annual tropospheric  $\text{NH}_3$   
188 concentration and several independent variables at  $0.25^\circ$  resolution: population density,  
189 livestock density, and cropped area. We calculated population density based on the 2017  
190 version of the US Department of Energy's Gridded Landscan population dataset (Dobson et  
191 al., 2000; available at <https://landscan.ornl.gov>). Livestock density was based on the FAO  
192 global gridded livestock dataset for the year 2007 (Robinson et al., 2014). Before analysis,  
193 we converted the livestock densities of chickens, goats, pigs, and sheep to tropical livestock  
194 units (TLU), using values of 0.01, 0.1, 0.2, and 0.1 TLU, respectively; North African cattle  
195 were converted using a factor of 0.7, whereas sub-Saharan cattle were converted using a  
196 factor of 0.5 (Chilonda and Otte, 2006). For cropped area, we used the MODIS MCD12C1  
197 (collection 5) land cover product as described above. We conducted spatial analyses by  
198 establishing a map of  $1.5^\circ$  grid cells and calculating the correlation between the value of  
199 each independent variable and  $\text{NH}_3$  for all  $0.25^\circ$  grid cells within the larger grid cells ( $N =$   
200 144 including water grid cells, though these were excluded from the analysis).

201

202 National data on annual livestock numbers, crop production, and fertilizer N use were  
203 obtained from the UN Food and Agriculture Organization FAOSTAT for 51 African countries  
204 (FAO, 1998). Livestock data consisting of sheep, goats, cattle, and pigs were converted to  
205 tropical livestock units as described above, and buffaloes were converted using a conversion  
206 factors of 0.7 (Chilonda and Otte, 2006). National-level mean annual cropland area, burned



207 area, and atmospheric NH<sub>3</sub> and CO concentrations were also calculated for each of the 51  
208 countries from the spatial datasets described above. Countries were sorted into three bins  
209 based on whether their relative change in mean annual NH<sub>3</sub> concentration was low, medium  
210 or high, and means and standard errors were calculated for each of the three 17-country  
211 bins.

212 Linear trend analyses were conducted using linregress from the scipy.stats package  
213 in Python v3.6.3. Statistical analyses of national scale data were conducted using ANOVA in  
214 R. Data were log transformed when necessary to meet the assumptions of ANOVA, and in  
215 cases where assumptions were not met following transformations, the Kruskal-Wallis test  
216 was used. Values of  $\alpha$  for treatment comparisons following significant ANOVA results were  
217 corrected for multiple testing using Benjamini-Hochberg corrections.

218  
219

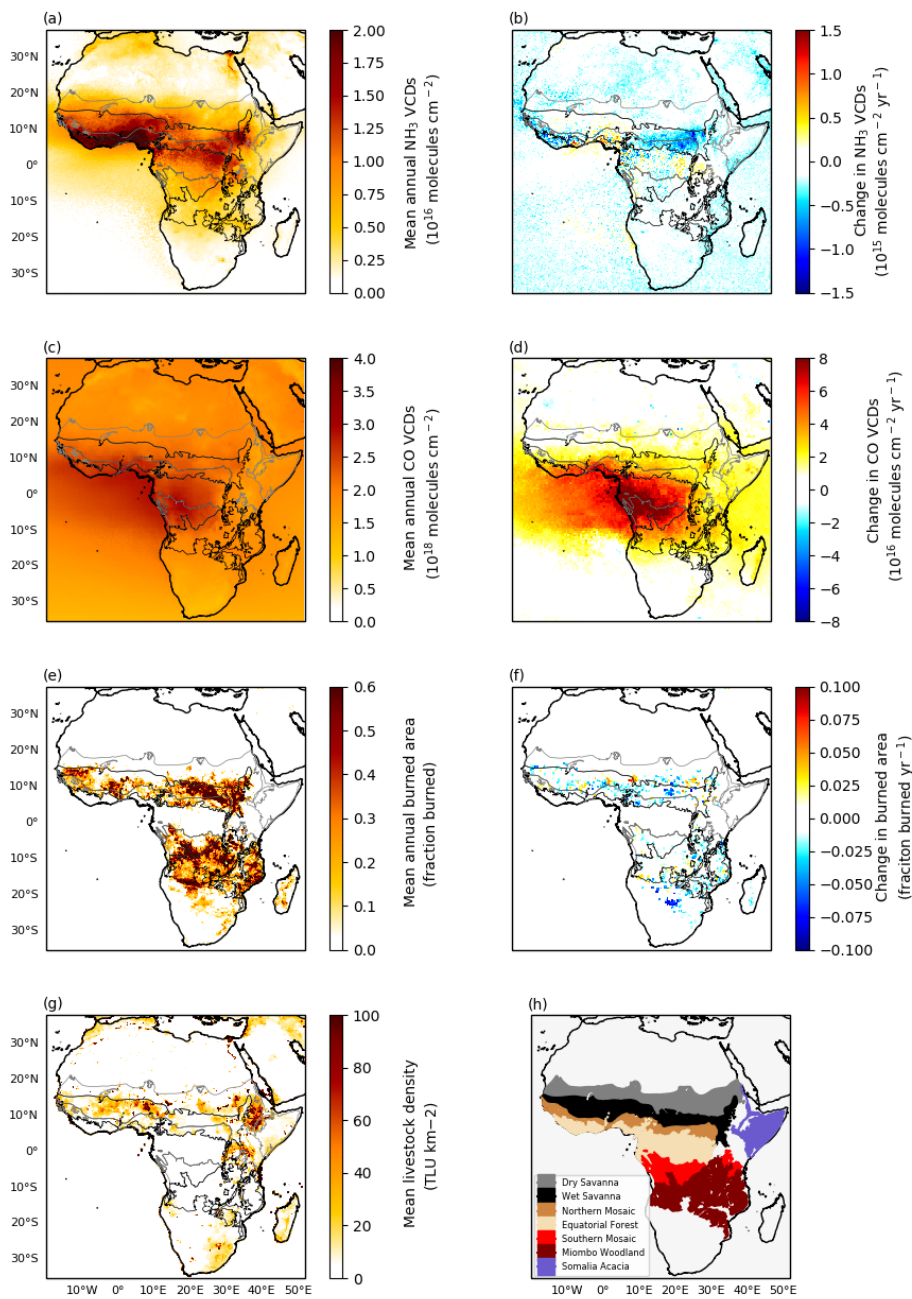
### 220 **3. Results & Discussion**

#### 221 **3.1 Continental distributions and trends**

222 Mean annual NH<sub>3</sub> concentrations for 2008-2017 are highest across the savannas  
223 and forest-savanna mosaics in North equatorial Africa, and especially in West Africa; there  
224 are smaller regional hotspots in the Lake Victoria basin and along the Nile delta and river  
225 (Fig. 1a). Parts of these regions experience substantial biomass burning (Fig. 1e), high  
226 livestock densities (Fig. 1g), and or high cropland cover (Fig. S1), all of which can  
227 contribute to NH<sub>3</sub> emissions. The high concentrations in West Africa, which is one of the  
228 major global NH<sub>3</sub> hotspots (Van Damme et al., 2018), is likely the result of biomass burning  
229 emissions. Biomass burning emissions tend to drive seasonal variation in NH<sub>3</sub> VCDs in  
230 West Africa, with the largest emissions occurring late in the dry season and early rainy  
231 season (Hickman et al., *in review*). In addition to local emissions, biomass burning  
232 emissions and their reactive products are transported to the coast of West Africa during  
233 both the northern hemisphere rainy season, when it is transported from central and  
234 southern Africa, and during the dry season, when it is transported from biomass burning  
235 regions to the east (Sauvage et al., 2007).

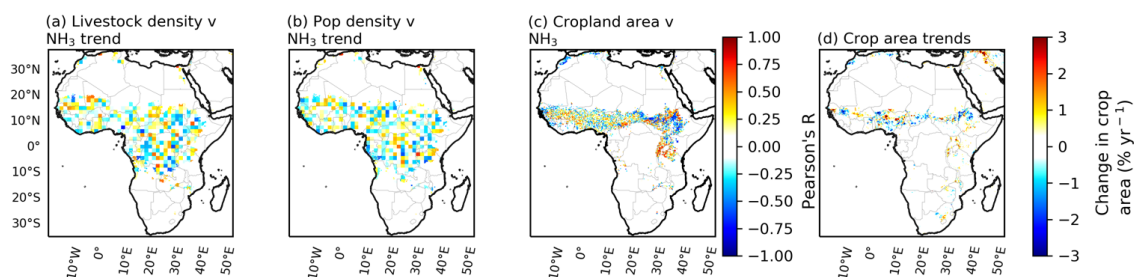


236            In addition to being hotspots of mean  $\text{NH}_3$  concentrations, some of these regions  
237 have also experienced increases in  $\text{NH}_3$  concentrations from 2008 to 2017 (Fig. 1d). Like  
238 Warner et al. (2017), we observed some increases in the northern grasslands and Nile  
239 region, but we also observe trends in the Lake Victoria Basin, which Warner et al. (2017)  
240 did not. We also do not observe consistent changes over central African forests, where  
241 Warner et al. (2017) observed substantial increases in  $\text{NH}_3$  VCDs. Also in contrast to  
242 Warner et al. (2017), we observe a prominent decline in  $\text{NH}_3$  VCDs over South Sudan (Fig.  
243 1b). We evaluate several of these regions in more detail below.



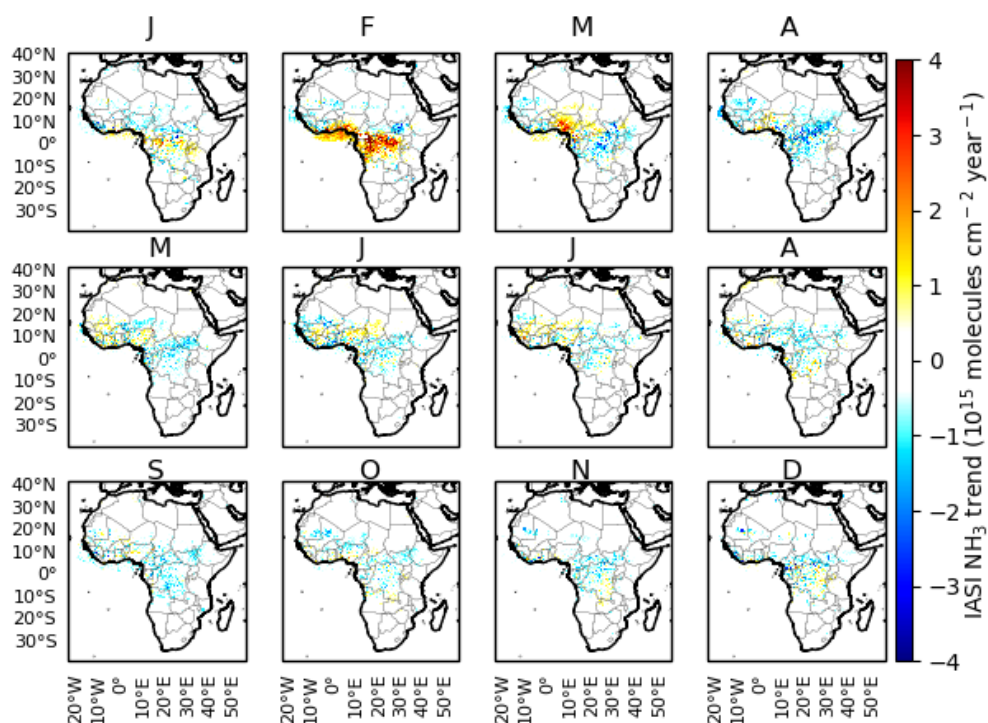


245 **Figure 1.** Livestock density and annual averages and trends in burned area and  
246 atmospheric  $\text{NH}_3$  concentrations across seven sub-Saharan African ecoregions. Mean  
247 annual (a) and trend (b) in atmospheric  $\text{NH}_3$  VCDs from IASI for the period 2008 through  
248 2017. Mean annual (c) and trend (d) in annual atmospheric CO VCDs from IASI for the  
249 same period. Mean annual (e) and trend (f) in annual burned area from MODIS for 2008-  
250 2017. Livestock densities for 2007 from the FAO (f), and key for the outlines of seven  
251 major African ecoregions (g).



253 **Figure 2.** Spatial correlations between mean annual atmospheric  $\text{NH}_3$  concentrations and  
254 livestock density (a), population density (b), and mean cropland area (c), as well as trend in  
255 crop area for 2008 through 2016 (d). In correlations,  $\text{NH}_3$  trend is based on data for 2008  
256 through 2017, livestock density data are for the year 2007, population density data are for  
257 the year 2017, and cropland area are the mean of 2008 through 2016.

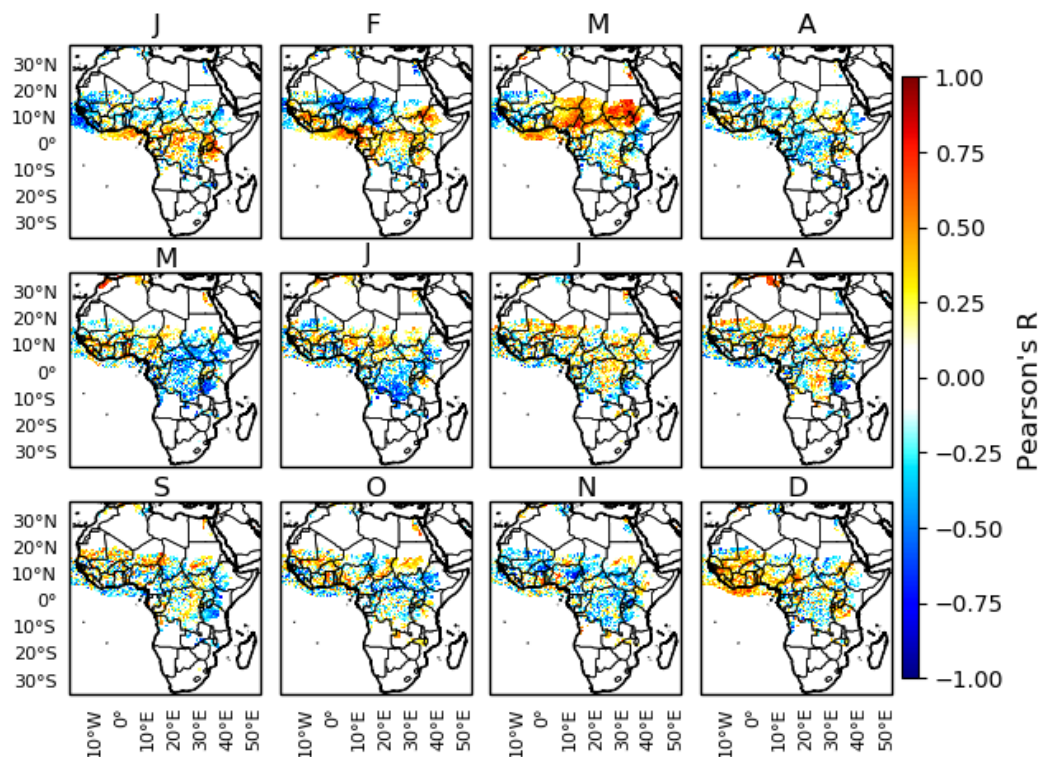
258



259

260 **Figure 3.** Change in mean monthly atmospheric NH<sub>3</sub> VCDs for the period 2008 through  
261 2017.

262



263

264

265 **Figure 4.** Correlation coefficient for the relationship between mean annual CO and  
266 NH<sub>3</sub> VCDs over 2008 through 2017. Regions where mean annual NH<sub>3</sub> VCDs for the entire  
267 period are under  $5 \times 10^{15}$  molecules cm<sup>-2</sup> are screened out.

268

### 269 **3.2 West Africa**

270 The increasing trend in NH<sub>3</sub> VCDs over West Africa are centered over Nigeria and  
271 the southern coast, and to a lesser extent across parts of the wet savanna (Fig. 1b). The  
272 spatial distribution of the mean annual NH<sub>3</sub> trend is overlapped by a substantial increase in  
273 mean annual CO VCDs (Fig. 1b, 1d), pointing to a biomass burning source. Earlier studies  
274 have found substantial declines in annual burned area across the north equatorial African



275 biomass burning region as detected by MODIS (Andela et al., 2017; Andela and Van Der  
276 Werf, 2014) and related declines in NO<sub>2</sub> VCDs across the region (Hickman et al., *in review*),  
277 which would seem to stand in contrast to the increasing CO and NH<sub>3</sub> trends observed here.  
278 However, the annual decline in burned area and NO<sub>2</sub> VCDs is characterized by  
279 heterogeneity when considering individual months: during the transition between the dry  
280 and rainy seasons, both NO<sub>2</sub> VCDs and burned area exhibit increasing rather than  
281 decreasing trends in West Africa (Hickman et al., *in review*). Although these increases are  
282 small in the annual context, they occur at a time of year when biomass burning combustion  
283 is less complete, leading to greater emissions of less oxidized species such as CO and NH<sub>3</sub>,  
284 rather than the more fully oxidized species such as CO<sub>2</sub> and NO<sub>2</sub> that dominate emissions  
285 during the peak of the biomass burning season (Hickman, et al., *in review*; Zheng et al.,  
286 2018). Indeed, our observations suggest that much of the increasing NH<sub>3</sub> trend occurs  
287 during this transitional period, with NH<sub>3</sub> VCDs increasing by roughly 6% yr<sup>-1</sup> for all of  
288 Nigeria during February and March (Fig. 3). Variation in NH<sub>3</sub> VCDs are positively  
289 correlated with CO VCDs (Fig. 4), which are also increasing during this period (Fig. S2).  
290 These correlations imply a biomass burning source for the increasing NH<sub>3</sub> VCDs in West  
291 Africa. It is unlikely that changes in chemical sinks—specifically, the formation of nitrate  
292 aerosols in reactions with NO<sub>x</sub> or sulfate—are responsible for the trend: the observed  
293 increase in NO<sub>2</sub> VCDs observed during February and March would be expected to lead to a  
294 shorter NH<sub>3</sub> lifetime and lower VCDs. In addition, emissions of SO<sub>2</sub> are relatively low in  
295 West Africa, with moderate emissions occurring in Nigeria, but neither emissions nor  
296 lifetime exhibit clear seasonal variation (Lee et al., 2011).

297 Small agricultural fires are likely an important contributor to the increasing NH<sub>3</sub>  
298 VCDs during the dry-to-rainy season transitional period—a period when agricultural fires  
299 are common in the region (Korontzi et al., 2006). There are large numbers of small fires  
300 that are not detected by MODIS during these months: estimates of burned area during  
301 February, March, and April are revised upwards by roughly a factor of 3 to 6 over MODIS  
302 when small fires are included (Roteta et al., 2019). Many of these small fires are likely  
303 related to agricultural field preparation prior to planting (Gbadegesin and Olusesi, 1994),  
304 which typically takes place in March or April (Vrieling et al., 2011; Yegbemey et al., 2014).  
305 An increase in fires during this transitional period is also consistent with one of the



306 primary mechanisms behind the overall decline in burned area: roughly half of the decline  
307 is attributed to increased population density and the expansion of agricultural area, which  
308 contributes to the anthropogenic suppression of larger fires (Andela et al., 2017; Andela  
309 and Van Der Werf, 2014). This agricultural expansion, however, can be expected to be  
310 accompanied by increases in small fires used for the removal of stubble or harvest  
311 byproduct (Gbadegesin and Olusesi, 1994), leading to the increased emissions during the  
312 rainy-to-dry season transition observed here.

313 Globally, agricultural emissions from fertilized soils and livestock excreta are the  
314 largest source of  $\text{NH}_3$  (Bauer et al., 2016), and Warner et al. (Warner et al., 2017) suggest  
315 that national-scale changes in fertilizer use could explain the  $\text{NH}_3$  trend over Nigeria.  
316 However, as noted above, much of the increase in West Africa occurs prior to the start of  
317 the planting season—before fertilizer is applied—and appears likely to be due to biomass  
318 burning emissions instead. Fertilizer or manure may make a contribution to the increasing  
319 trend later in the year, as  $\text{NH}_3$  VCDs increase in the wet savanna during May, June, and July  
320 (Fig. 3), though there are also significant correlations between  $\text{NH}_3$  and CO VCDs (Fig. 4),  
321 suggesting that biomass burning may continue to play an important role. However, average  
322 N fertilizer use in West Africa is universally under  $40 \text{ kg N ha}^{-1}$ , typically under  $20 \text{ kg N ha}^{-1}$ ,  
323 and is under  $10 \text{ kg N ha}^{-1}$  in Nigeria—over an order of magnitude lower than rates in  
324 Europe, the United States, and China (FAO, 1998). Although percentage changes in  
325 fertilizer use are substantial, in absolute terms they represent increases of less than  $2 \text{ kg N}$   
326  $\text{ha}^{-1} \text{ yr}^{-1}$ , and frequently less than  $1 \text{ kg N ha}^{-1} \text{ yr}^{-1}$ , a relatively small but perhaps not entirely  
327 trivial perturbation to the N cycle. Between 2000 and 2007, total N deposition averaged  
328  $8.38 \text{ kg N ha}^{-1} \text{ yr}^{-1}$  in wet savanna and  $14.75 \text{ kg N ha}^{-1} \text{ yr}^{-1}$  in forest ecosystems based on  
329 surface sampling sites (Galy-Lacaux and Delon, 2014), and biological N fixation in tropical  
330 and wet savannas has been estimated as ranging from  $16$  to  $44 \text{ kg N ha}^{-1} \text{ yr}^{-1}$  (Bustamante  
331 et al., 2006), suggesting that fertilizer increases may represent a 1 to 2% annual increase in  
332 N inputs. But given the small magnitude of fertilizer applications, it appears unlikely that  
333 changes in fertilizer use can explain the entirety of  $\text{NH}_3$  increases during the growing  
334 season.

335



### 336            **3.3. South Sudan**

337            The most notable declining trend in  $\text{NH}_3$  VCDs occurs in South Sudan, at a rate of  
338 over  $2\% \text{ yr}^{-1}$  during the February through May period (Fig. 1b). It appears that this decline  
339 is related to interannual variation in the flooded extent of the Sudd, a vast wetland that  
340 connects the White and Blue Nile tributaries. Seasonal variation of inflow to the Sudd leads  
341 to variation in flooded extent: an area of roughly  $15,000 \text{ km}^2$  is permanently flooded, and  
342 another roughly  $15,000 \text{ km}^2$  is temporarily flooded each year, with considerable  
343 interannual variation in the total flooded area (Di Vittorio and Georgakakos, 2018). Among  
344 other factors, drying soils should increase production and emissions of  $\text{NH}_3$  from soils, as  
345 Eq. 1 is shifted to the right (Clarisse et al., 2019). Earlier work evaluating an  $\text{NH}_3$  hotspot  
346 over Lake Natron in Tanzania found that the drying of seasonally flooded soils leads to  
347 large emissions of  $\text{NH}_3$ : As the waters of Lake Natron recede during the dry season each  
348 year and the surrounding mud flats dry out,  $\text{NH}_3$  VCDs increase rapidly, with hotspots  
349 appearing over the mudflats (Clarisse et al., 2019). These elevated VCDs are attributed to  
350 multiple factors, including the effects of drying on concentrations of  $\text{NH}_3$  in solution (which  
351 increases the concentration gradient with the atmosphere), reduced biological uptake of  
352  $\text{NH}_3$ , convective transport of dissolved  $\text{NH}_3$  from depth to the soil surface, and increased  
353 mineralization of labile organic matter (Clarisse et al., 2019).

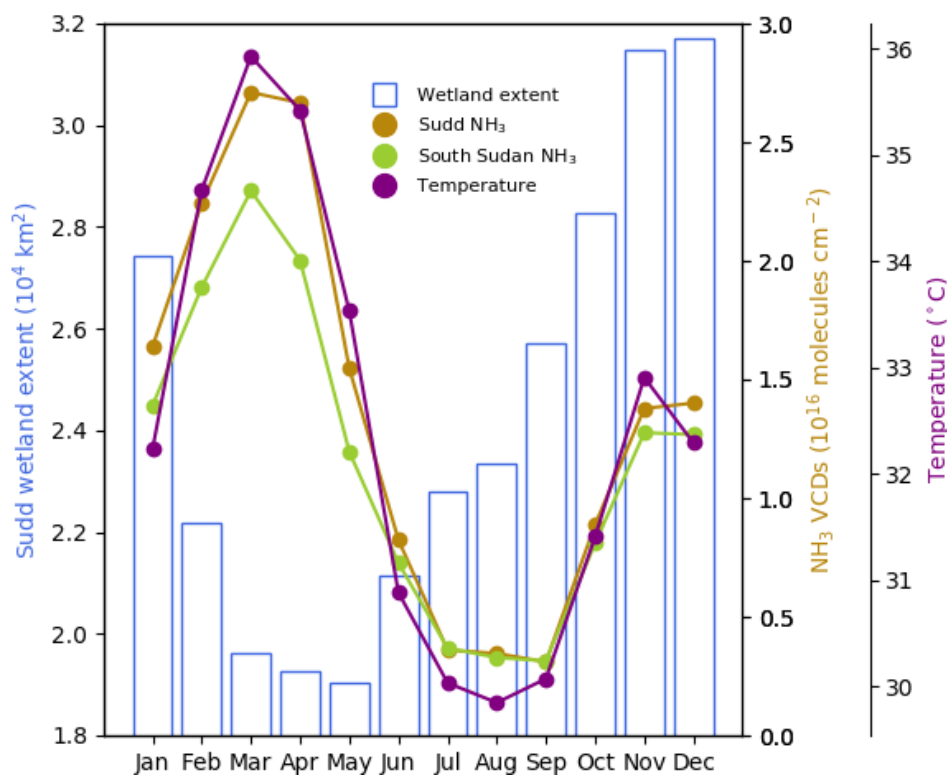
354            We find the same clear seasonal relationship between wetland flooded extent and  
355  $\text{NH}_3$  concentrations over the Sudd—VCDs increase as waters recede from the temporarily  
356 flooded area, leading to annual maxima from February through May (Fig. 5; bounding box  
357 of  $29\text{E}$  to  $31.5\text{E}$  and  $6\text{N}$  to  $9.9\text{N}$ ). Like the entire country, seasonal variation in  $\text{NH}_3$  VCDs  
358 over the Sudd follow variation in surface temperature, but  $\text{NH}_3$  concentrations over the  
359 Sudd are substantially elevated compared to surrounding regions during this time of year  
360 but not others, suggesting that an additional mechanism is contributing to the elevated  
361 emissions in the Sudd during February through May, a period that spans the end of the dry  
362 season and start of the rainy season (Fig. S3). This conclusion is supported by an analysis  
363 of interannual variation of VCDs during the February through May period. Interannual  
364 variation in  $\text{NH}_3$  VCDs is largely decoupled from variation in temperature, but  $\text{NH}_3$  VCDs



365 appear to vary inversely with the amount of area that dries out each year (Fig. 6). Over the  
366 period for which flooded extent data are currently available for the Sudd, the minimum  
367 flooded extent tends to increase—that is, less area dries out each year—resulting in an  
368 overall decline in  $\text{NH}_3$  VCDs. Linear regression reveals that this change in flooded extent  
369 explains a large proportion of the variation in  $\text{NH}_3$  in the Sudd bounding box ( $r=-0.69$ ,  
370  $p=0.03$ ) as well as for the country as a whole ( $r=-0.70$ ,  $p=0.02$ ) during February through  
371 May. These analyses strongly suggest that the declining trend in  $\text{NH}_3$  over the Sudd is a  
372 direct result of an overall increase in the minimum flooded extent over the observation  
373 period.

374

375

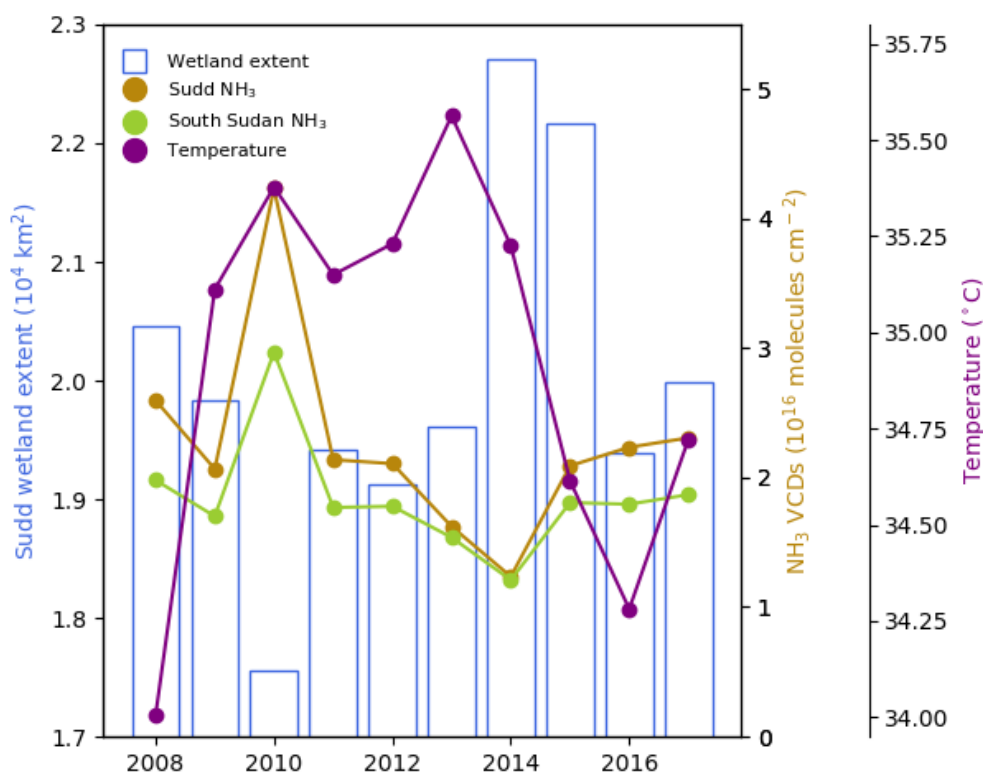


376



377 **Figure 5.** Mean monthly flooded extent of the Sudd, surface temperatures over  
378 South Sudan, and  $\text{NH}_3$  VCDs over the Sudd and the entirety of South Sudan for the period  
379 2008 through 2017.

380



381 **Figure 6.** February through May mean flooded extent of the Sudd, surface  
382 temperatures over South Sudan, and  $\text{NH}_3$  VCDs over the Sudd and the entirety of South  
383 Sudan for 2008 through 2017.

384

385  
386 It is possible that conflict in South Sudan could contribute to the decline in  $\text{NH}_3$   
387 VCDs. In 2013, a civil conflict emerged in South Sudan that was ultimately responsible for  
388 the displacement of millions of people (Global Internal Displacement Monitoring Centre,  
389 2020; World Bank, 2019) and the disruption of livestock migration patterns (Idris, 2018).



390 These disruptions could be expected to lead to a decrease in  $\text{NH}_3$  VCDs if they result in  
391 lower rates of fertilizer use and a decrease in livestock and livestock-related emissions.  
392 Although there are some spatial correspondences between the location of conflict events  
393 and changes in  $\text{NH}_3$  VCDs (Fig. S4), the change in  $\text{NH}_3$  VCDs appears already to have been  
394 underway years in advance of the onset of conflict (Fig. 6, Fig. S5), suggesting that other  
395 factors are responsible for the interannual variation. Displacement spiked in 2014, the year  
396 that  $\text{NH}_3$  VCDs were at their lowest values. It is possible that this displacement and the  
397 associated conflict contributed to the low  $\text{NH}_3$  values, but 2014 was the year of the largest  
398 Sudd extent during February through May, which would also be expected to reduce  $\text{NH}_3$   
399 emissions. The number of refugees and internally displaced people increased substantially  
400 from 2013 through 2017, a period during which the dry season flooded extent of the Sudd  
401 decreased, and  $\text{NH}_3$  VCDs increased (Fig. S5). Maps of annual mean  $\text{NH}_3$  VCDs over the IASI  
402 lifetime reveal that a large amount of the interannual variability occurs over the Sudd (Fig.  
403 S6), though there is also variability in other parts of the country, though these do not map  
404 strongly to interannual variability in precipitation (Fig. S7). The strong spatial relationship  
405 between the Sudd and interannual  $\text{NH}_3$  variability suggests that Sudd flooded extent is  
406 likely the main factor responsible for the interannual variation in  $\text{NH}_3$  VCDs during this  
407 period, and the overall trend we observe for 2008 through 2017.

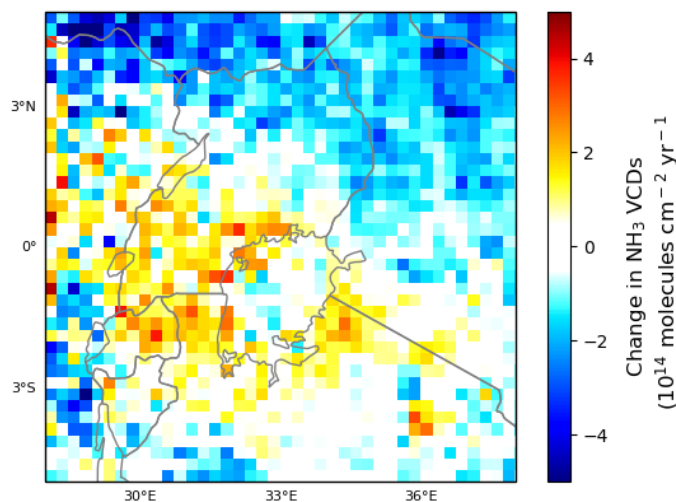
408 It is unlikely that changes in chemical sinks are responsible for the decline in  $\text{NH}_3$   
409 VCDs. VCDs of tropospheric  $\text{NO}_2$  are also decreasing in the region (Fig. S8), which is  
410 suggestive of less formation of particulate-phase ammonium rather than more.  
411 Anthropogenic  $\text{SO}_2$  emissions in Africa in general and South Sudan in particular are very  
412 low (European Commission Joint Research Centre (JRC)/Netherlands Environmental  
413 Assessment Agency (PBL), 2016), and would not be expected to be emitted from the Sudd;  
414 more generally, the clear spatial association between the  $\text{NH}_3$  trend and the Sudd (Fig. 1,  
415 Fig. S6) is strongly suggestive of changes in emissions rather than atmospheric processes  
416 being responsible for the trend.

417

### 418 **3.4 Lake Victoria Basin region**



419           The Lake Victoria Basin and its surroundings—an area including elevated mean NH<sub>3</sub>  
420 VCDs—exhibit an increasing NH<sub>3</sub> trend (Fig. 1b, Fig. 7, Fig. S9), which appears to be the  
421 result of increasing agricultural activity in the area. The region includes a high and  
422 increasing density of agricultural land (Fig. 2d, Fig. S1, Fig. S10), and these increases in  
423 cropped area are positively correlated with increases in NH<sub>3</sub> VCDs across much of the  
424 region (Fig. 2c). The northern and southern halves of the Lake Victoria region have distinct  
425 growing seasons: in the north, the season generally starts in April, whereas in the south, it  
426 starts in November or December (Vrieling et al., 2011). The long-term trend reflects this  
427 seasonality, with increases in the north and south occurring during their respective  
428 growing seasons (Fig. 3). Fertilizer use in Lake Victoria region is low: national averages  
429 range from about 1 to 3 kg nutrients ha<sup>-1</sup> in Uganda to about 35 to 40 kg nutrients ha<sup>-1</sup> in  
430 Kenya; to put these numbers in context, Organization for Economic Cooperation and  
431 Development (OECD) countries use about 135-140 kg nutrients ha<sup>-1</sup> (World Bank, 2019).  
432 Although rates of fertilizer use have increased by substantial proportions, the absolute  
433 amount of increase is relatively small, typically roughly 1 to 10 kg nutrients decade<sup>-1</sup>.  
434 Unlike in West Africa, however, interannual variation in burned area (Fig. S11) does not  
435 exhibit a clear relationship with changes in NH<sub>3</sub> VCDs. Consequently, we expect that both  
436 the expansion and intensification of agriculture in the region contribute to the increasing  
437 NH<sub>3</sub> VCDs.



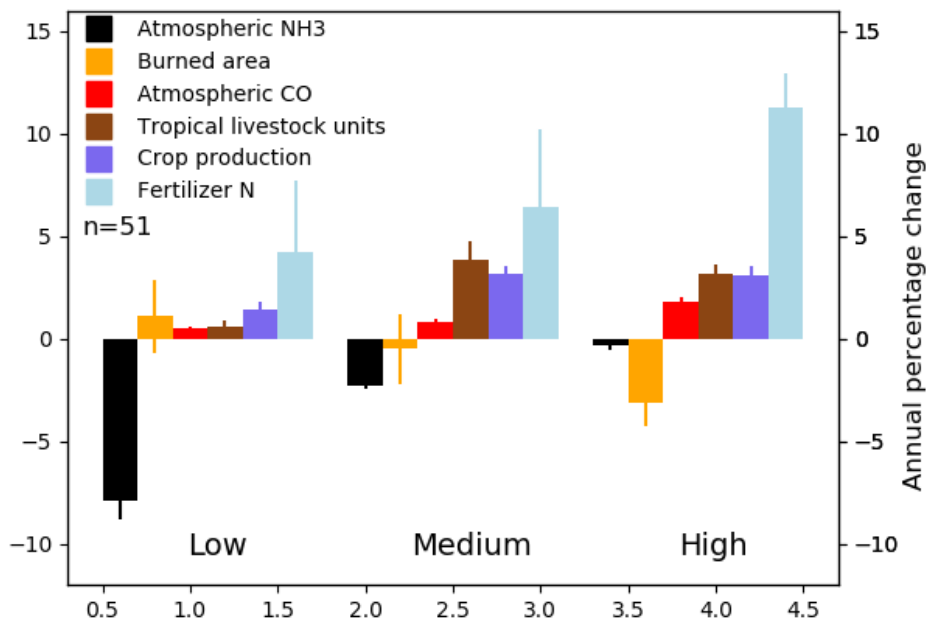
438

439 **Figure 7.** Change in mean annual NH<sub>3</sub> VCDs over the Lake Victoria region, 2008  
440 through 2017.

441

### 442 3.5 National-scale relationships

443 Examining relationships at a national scale can provide insight into relationships  
444 between changes in agricultural or biomass burning and changes in atmospheric NH<sub>3</sub> VCDs  
445 at larger scales. When grouping countries into three bins based on their annual percentage  
446 changes in NH<sub>3</sub> VCDs, a broad relationship between agriculture and NH<sub>3</sub> VCDs becomes  
447 apparent (Fig. 8). The rate of change in national-scale NH<sub>3</sub> VCDs varies significantly among  
448 bins ( $p < 0.001$ ), though in no bins is the rate of change positive. The annual percentage  
449 changes of national gross production ( $p = 0.009$ ) and livestock in TLUs ( $p = 0.003$ ) vary  
450 significantly by bin, whereas annual percentage changes in fertilizer N use are not quite  
451 significantly different across bins ( $p = 0.18$ ). Nevertheless the general pattern suggests that  
452 countries with greater agricultural activity tend to have smaller declines in NH<sub>3</sub> VCDs.  
453



454  
455 **Figure 8.** Annual percentage changes in national mean annual NH<sub>3</sub> VCDs, burned area, CO,  
456 livestock, crop yield, and fertilizer N use for African countries with low, medium, or high  
457 rates of NH<sub>3</sub> VCD change. Error bars represent the standard error of the mean. See Table  
458 S1 for the list of countries in each bin.

459  
460

461 In addition to these direct agricultural relationships, there is also a possibility that  
462 changes in biomass burning are associated with changes in NH<sub>3</sub> VCDs. Although the  
463 differences in the annual percentage change in burned area were not significant among  
464 bins ( $p=0.61$ ), the overall pattern is consistent with earlier results finding that a reduction  
465 in burned area across the northern biomass burning region was associated in part with the  
466 expansion of agriculture and presumed anthropogenic suppression of fire (Andela et al.,  
467 2017; Andela and Van Der Werf, 2014). Indeed, many of the countries in the high bin—  
468 where burned area exhibits a declining trend—are from that biomass burning region  
469 (Table S1). However, burned area as measured by MODIS is likely an imperfect predictor



470 for  $\text{NH}_3$  emissions—MODIS underestimates burned area by a factor of 3 to 6 during  
471 shoulder seasons (Roteta et al., 2019), which is when fires are expected to emit more  
472 reduced species such as  $\text{NH}_3$  (Zheng et al., 2018). In contrast to burned area, the annual  
473 change in column densities of CO—which tends to be co-emitted with  $\text{NH}_3$  from fires—  
474 differed significantly among bins ( $p < 0.0001$ ) and was significantly higher in the high bin  
475 than in the low or medium bins. ( $p < 0.001$ , post-hoc tests). The higher annual CO changes  
476 in the high bin could be related to larger anthropogenic fossil fuel emissions, but we see no  
477 difference among bins in per capita GDP growth rates ( $p = 0.24$ ); such a difference would be  
478 expected if differences in economic development were responsible for the CO differences.  
479 These results leave open the possibility that changes in either biofuel emissions or biomass  
480 burning emissions—perhaps from smaller fires not observed in the MODIS burned area  
481 product—may be primarily responsible for the difference in CO between bins.

482

#### 483 **4. Conclusion**

484 Using IASI, we have observed both increases and decreases in atmospheric  $\text{NH}_3$   
485 VCDs in different regions in Africa between 2008 and 2017, with different factors affecting  
486 trends in different regions.

487 We observed increases in  $\text{NH}_3$  VCDs in West Africa, which earlier work had  
488 concluded was likely related to increased fertilizer use. Fertilizer is not typically applied in  
489 West Africa until the start of the growing season—often April—but we find that most of the  
490  $\text{NH}_3$  increase occurs during February and March, suggesting that increasing fertilizer use is  
491 unlikely to provide a complete explanation for the  $\text{NH}_3$  trend. Agriculture may  
492 nevertheless play a role, with enhanced burned area and especially CO concentrations in  
493 February suggestive of increased burning of crop stubble in preparation for planting during  
494 this time of year. Fires in this region tend to emit a greater proportion of less oxidized  
495 species such as  $\text{NH}_3$  at the end of the dry season, consistent with a biomass burning source  
496 for the increasing  $\text{NH}_3$  VCDs.

497 Decreases in  $\text{NH}_3$  VCDs were largest in South Sudan, especially over the Sudd  
498 wetland, where  $\text{NH}_3$  VCDs vary seasonally with the extent of area flooded. As the  
499 temporarily flooded areas of the Sudd dry out each year,  $\text{NH}_3$  VCDs increase as reduction in  
500 soil moisture drives increased production and volatilization of  $\text{NH}_3$ . The area of the Sudd



501 that is flooded each year varies, and from 2008 through 2014, the area that remains  
502 flooded during the dry season generally increased. This increase in the dry season flooded  
503 area drove a decrease in  $\text{NH}_3$  VCDs: with less soil drying out, the seasonal maxima in  $\text{NH}_3$   
504 VCDs were lower. Although it is possible that conflict in South Sudan could contribute to  
505 changes in  $\text{NH}_3$  VCDs, the timing and distribution of conflict events and human  
506 displacement suggest that other factors are likely more important.

507 Modest increases in  $\text{NH}_3$  VCDs were observed in the Lake Victoria region. This  
508 region has experienced increases in agricultural area during the IASI observation period,  
509 and these changes explained a large proportion of the variation in  $\text{NH}_3$  VCDs across large  
510 patches of the region, where biomass burning could not. We expect that both expansion  
511 and intensification of agriculture in this region could contribute to the positive  $\text{NH}_3$  trend.

512 Considering national-scale statistics, most countries showed an overall decline in  
513 mean annual  $\text{NH}_3$  VCDs over the observation period. Comparisons between equally sized  
514 bins of 17 countries each revealed an inverse relationship between  $\text{NH}_3$  VCDs and rates of  
515 change in agricultural variables such as livestock, crop production, and (though not quite  
516 significant) N fertilizer use—generally, greater rates of increase in agricultural variables  
517 were associated with smaller decreases in  $\text{NH}_3$  VCDs.

518 However, even though fertilizer use has been increasing in sub-Saharan Africa, it  
519 remains extremely low relative to other continents, and relative to the levels needed to  
520 attain food security. Average fertilizer use in most countries in the region is under 20 kg N  
521  $\text{ha}^{-1}$ , and sometimes less than 5 kg N  $\text{ha}^{-1}$ . Although recommended fertilizer rates are lower  
522 in most African countries than in the U.S. or Europe, increasing N inputs to 50, 100, or 150  
523 kg N  $\text{ha}^{-1}$  represents a major perturbation to the regional N cycle, and potentially a large  
524 new source of  $\text{NH}_3$  to the atmosphere. West Africa is already a global  $\text{NH}_3$  hotspot (Van  
525 Damme et al., 2018), suggesting that encouraging policies that can help to limit  $\text{NH}_3$   
526 emissions during the early stages of agricultural intensification in Africa may help mitigate  
527 potential impacts on the atmosphere. Fortunately, agricultural practices such as sub-  
528 surface application of fertilizer, which is already being promoted to smallholder farmers,  
529 can serve to both limit  $\text{NH}_3$  emissions also help to increase crop yields.

530 These past and anticipated future trends also make the case for expanding capacity  
531 for atmospheric monitoring in sub-Saharan Africa. Although long-term monitoring



532 networks have been established in West Africa (Adon et al., 2010; Ossohou et al., 2019) and  
533 South Africa (Conradie et al., 2016), the spatio-temporal resolution of surface  
534 measurements is very coarse when compared to the data available in other parts of the  
535 world, and will limit our ability to understand how agricultural and socio-economic  
536 development in Africa affect the atmosphere. Satellite observations can help to bridge  
537 some of these data gaps, but have their own spatio-temporal limitations, and would further  
538 benefit from additional high-quality surface observations for evaluation of retrieval  
539 products.

540

541 **Data availability:** All data used in this study are available from public sources, with the  
542 exception of Sudd wetland extent, which is available by request from Courtney Di Vittorio. The  
543 IASI NH<sub>3</sub> and CO data are available from The IASI <https://iasi.aeris-data.fr>. The NOAA Global  
544 Surface Temperature Dataset is available at [https://data.nodc.noaa.gov/cgi-](https://data.nodc.noaa.gov/cgi-bin/iso?id=gov.noaa.ncdc:C01585)  
545 [bin/iso?id=gov.noaa.ncdc:C01585](https://data.nodc.noaa.gov/cgi-bin/iso?id=gov.noaa.ncdc:C01585). MODIS burned area data are available from  
546 <https://www.globalfireshdata.org/data.html>. MODIS agricultural area are available at  
547 <https://lpdaac.usgs.gov/products/mcd12c1v006/>. TRMM 3B42 precipitation data are available  
548 from <https://pmm.nasa.gov/data-access/downloads/trmm>. The Gridded Livestock of the World  
549 data are available from <https://livestock.geo-wiki.org/home-2/>. Population density data for 2017  
550 are available at <https://landscan.ornl.gov/downloads/2017>. FAO national crop production and  
551 fertilizer N data are available at <http://www.fao.org/faostat/en/>. Data on conflict events from  
552 ACLED are available at <https://acleddata.com/#/dashboard>. World Bank national statistics  
553 on refugees and internally displaced people are available at <https://data.worldbank.org>.

554

555 **Author Contribution:** J.E.H. designed the study, conducted the analysis, and wrote the paper.  
556 NA, ED, CD, MO, CG-L, KT, and SEB contributed to study design and edited the paper. LC, P-  
557 FC, and MVD developed the original IASI trace gas retrievals and edited the paper.

558 The authors declare that they have no conflict of interest.

559



## 560 **References**

- 561 van der A, R. J., Eskes, H. J., Boersma, K. F., van Noije, T. P. C., Van Roozendaal, M., De Smedt,  
562 I., Peters, D. H. M. U. and Meijer, E. W.: Trends, seasonal variability and dominant NO<sub>x</sub>  
563 source derived from a ten year record of NO<sub>2</sub> measured from space, *J. Geophys. Res.*  
564 *Atmos.*, 113(4), D04302, doi:10.1029/2007JD009021, 2008.
- 565 Adon, M., Galy-Lacaux, C., Yoboué, V., Delon, C., Lacaux, J. P., Castera, P., Gardrat, E., Pienaar,  
566 J., Al Ourabi, H., Laouali, D., Diop, B., Sigha-Nkamdjou, L., Akpo, a., Tathy, J. P., Lavenu, F. and  
567 Mougín, E.: Long term measurements of sulfur dioxide, nitrogen dioxide, ammonia, nitric  
568 acid and ozone in Africa using passive samplers, *Atmos. Chem. Phys.*, 10(15), 7467–7487,  
569 doi:10.5194/acp-10-7467-2010, 2010.
- 570 AGRA: AGRA in 2008: Building on the New Momentum in African Agriculture., 2009.
- 571 Andela, N. and Van Der Werf, G. R.: Recent trends in African fires driven by cropland  
572 expansion and El Niño to la Niña transition, *Nat. Clim. Chang.*, 4(9), 791–795,  
573 doi:10.1038/nclimate2313, 2014.
- 574 Andela, N., Morton, D. C., Giglio, L., Chen, Y., Van Der Werf, G. R., Kasibhatla, P. S., DeFries, R.  
575 S., Collatz, G. J., Hantson, S., Kloster, S., Bachelet, D., Forrest, M., Lasslop, G., Li, F., Mangeon,  
576 S., Melton, J. R., Yue, C. and Randerson, J. T.: A human-driven decline in global burned area,  
577 *Science* (80-. ), 356(6345), 1356–1362, doi:10.1126/science.aal4108, 2017.
- 578 Anker, H. T., Baaner, L., Backes, C., Keessen, A. and Möckel, S.: Comparison of ammonia  
579 regulation in Germany, the Netherlands and Denmark – legal framework, Copenhagen.,  
580 2018.
- 581 Bauer, S. E., Tsigaridis, K. and Miller, R.: Significant atmospheric aerosol pollution caused by  
582 world food cultivation, *Geophys. Res. Lett.*, 43(10), 5394–5400,  
583 doi:10.1002/2016GL068354, 2016.
- 584 Behera, S. N., Sharma, M., Aneja, V. P. and Balasubramanian, R.: Ammonia in the  
585 atmosphere: A review on emission sources, atmospheric chemistry and deposition on  
586 terrestrial bodies, *Environ. Sci. Pollut. Res.*, 20(11), 8092–8131, doi:10.1007/s11356-013-  
587 2051-9, 2013.
- 588 Bouwman, A. F., Lee, D. S., Asman, W. A. H., Dentener, F. J., Van Der Hoek, K. W. and Olivier, J.  
589 G. J.: A global high-resolution emission inventory for ammonia, *Global Biogeochem. Cycles*,  
590 11(4), 561–587, 1997.



- 591 Bustamante, M. M. C., Medina, E., Asner, G. P., Nardoto, G. B. and Garcia-Montiel, D. C.:  
592 Nitrogen cycling in tropical and temperate savannas, *Biogeochemistry*, 79(1–2), 209–237,  
593 doi:10.1007/s10533-006-9006-x, 2006.
- 594 Cahoon, D. R., Stocks, B. J., Levine, J. S., Cofer, W. R. and O'Neill, K. P.: Seasonal distribution of  
595 African savanna fires, *Nature*, 359(6398), 812–815, doi:10.1038/359812a0, 1992.
- 596 Chen, L.-W. A., Verburg, P., Shackelford, A., Zhu, D., Susfalk, R., Chow, J. C. and Watson, J. G.:  
597 Moisture effects on carbon and nitrogen emission from burning of wildland biomass,  
598 *Atmos. Chem. Phys.*, 10(14), 6617–6625, doi:10.5194/acp-10-6617-2010, 2010.
- 599 Chilonda, P. and Otte, J.: Indicators to monitor trends in livestock production at national,  
600 regional and international levels, *Livest. Res. Rural Dev.*, 18(8), 1–12, 2006.
- 601 Clarisse, L., Clerbaux, C., Dentener, F., Hurtmans, D. and Coheur, P. F.: Global ammonia  
602 distribution derived from infrared satellite observations, *Nat. Geosci.*, 2(7), 479–483,  
603 doi:10.1038/ngeo551, 2009.
- 604 Clarisse, L., Van Damme, M., Gardner, W., Coheur, P.-F., Clerbaux, C., Whitburn, S., Hadji-  
605 Lazaro, J. and Hurtmans, D.: Atmospheric ammonia (NH<sub>3</sub>) emanations from Lake Natron's  
606 saline mudflats, *Sci. Rep.*, 9, 4441, doi:10.1038/s41598-019-39935-3, 2019.
- 607 Conradie, E. H., Van Zyl, P. G., Pienaar, J. J., Beukes, J. P., Galy-Lacaux, C., Venter, A. D. and  
608 Mkhathswa, G. V.: The chemical composition and fluxes of atmospheric wet deposition at  
609 four sites in South Africa, *Atmos. Environ.*, 146, 113–131,  
610 doi:10.1016/j.atmosenv.2016.07.033, 2016.
- 611 Van Damme, M., Wichink Kruit, R. J., Schaap, M., Clarisse, L., Clerbaux, C., Coheur, P. F.,  
612 Dammers, E., Dolman, A. J. and Erisman, J. W.: Evaluating 4 years of atmospheric ammonia  
613 (NH<sub>3</sub>) over Europe using IASI satellite observations and LOTOS-EUROS model results, *J.*  
614 *Geophys. Res.*, 119(15), 9549–9566, doi:10.1002/2014JD021911, 2014a.
- 615 Van Damme, M., Clarisse, L., Heald, C. L., Hurtmans, D., Ngadi, Y., Clerbaux, C., Dolman, A. J.,  
616 Erisman, J. W. and Coheur, P. F.: Global distributions, time series and error characterization  
617 of atmospheric ammonia NH<sub>3</sub> from IASI satellite observations, *Atmos. Chem. Phys.*, 14(6),  
618 2905–2922, doi:10.5194/acp-14-2905-2014, 2014b.
- 619 Van Damme, M., Whitburn, S., Clarisse, L., Clerbaux, C., Hurtmans, D. and Coheur, P. F.:  
620 Version 2 of the IASI NH<sub>3</sub> neural network retrieval algorithm: Near-real-time and  
621 reanalysed datasets, *Atmos. Meas. Tech.*, 10(12), 4905–4914, doi:10.5194/amt-10-4905-



- 622 2017, 2017.
- 623 Van Damme, M., Clarisse, L., Whitburn, S., Hadji-Lazaro, J., Hurtmans, D., Clerbaux, C. and  
624 Coheur, P.: Industrial and agricultural ammonia point sources exposed, *Nature*, 564, 99–  
625 103, 2018.
- 626 Dammers, E., Shephard, M. W., Palm, M., Cady-Pereira, K., Capps, S., Lutsch, E., Strong, K.,  
627 Hannigan, J. W., Ortega, I., Toon, G. C., Stremme, W., Grutter, M., Jones, N., Smale, D., Siemons,  
628 J., Hrpcek, K., Tremblay, D., Schaap, M., Notholt, J. and Willem Erisman, J.: Validation of the  
629 CrIS fast physical NH<sub>3</sub> retrieval with ground-based FTIR, *Atmos. Meas. Tech.*, 10(7), 2645–  
630 2667, doi:10.5194/amt-10-2645-2017, 2017.
- 631 Denier Van Der Gon, H. and Bleeker, A.: Indirect N<sub>2</sub>O emission due to atmospheric N  
632 deposition for the Netherlands, *Atmos. Environ.*, 39(32), 5827–5838,  
633 doi:10.1016/j.atmosenv.2005.06.019, 2005.
- 634 Dobson, J. E., Bright, E. A., Coleman, P. R., Durfee, R. C. and Worley, B. A.: A global population  
635 database for estimating populations at risk, *Photogramm. Eng. Remote Sens.*, 66(7), 849–  
636 857 [online] Available from: In Book..., 2000.
- 637 European Commission Joint Research Centre (JRC)/Netherlands Environmental  
638 Assessment Agency (PBL): Emission Database for Global Atmospheric Research (EDGAR),  
639 release version 4.3.1, 2016.
- 640 Fan, Y. and van den Dool, H.: A global monthly land surface air temperature analysis for  
641 1948-present, *J. Geophys. Res. Atmos.*, 113(1), D01103, doi:10.1029/2007JD008470, 2008.
- 642 FAO: FAO Statistics Database, FAOSTAT Stat. Database [online] Available from:  
643 <http://www.fao.org/faostat/en/> (Accessed 1 January 2019), 1998.
- 644 Friedl, M. A., McIver, D. K., Hodges, J. C. F., Zhang, X. Y., Muchoney, D., Strahler, A. H.,  
645 Woodcock, C. E., Gopal, S., Schneider, A., Cooper, A., Baccini, A., Gao, F. and Schaaf, C.: Global  
646 land cover mapping from MODIS: Algorithms and early results, *Remote Sens. Environ.*,  
647 83(1–2), 287–302, doi:10.1016/S0034-4257(02)00078-0, 2002.
- 648 Galy-Lacaux, C. and Delon, C.: Nitrogen emission and deposition budget in West and Central  
649 Africa, *Environ. Res. Lett.*, 9(12), doi:10.1088/1748-9326/9/12/125002, 2014.
- 650 Gbadegesin, A. and Olusesi, B. B.: Effects of land clearing methods on soil physical and  
651 hydrological properties in southwestern Nigeria, *Environmentalist*, 14(4), 297–303  
652 [online] Available from: <http://www.scopus.com/inward/record.url?eid=2-s2.0->



653 0022858519&partnerID=40&md5=3051b1dd91ff2990e37fe7466872923e, 1994.  
654 George, M., Clerbaux, C., Hurtmans, D., Turquety, S., Coheur, P. F., Pommier, M., Hadji-  
655 Lazaro, J., Edwards, D. P., Worden, H., Luo, M., Rinsland, C. and McMillan, W.: Carbon  
656 monoxide distributions from the IASI/METOP mission: Evaluation with other space-borne  
657 remote sensors, *Atmos. Chem. Phys.*, 9(21), 8317–8330, doi:10.5194/acp-9-8317-2009,  
658 2009.  
659 Giglio, L., Boschetti, L., Roy, D. P., Humber, M. L. and Justice, C. O.: The Collection 6 MODIS  
660 burned area mapping algorithm and product, *Remote Sens. Environ.*, 217, 72–85,  
661 doi:10.1016/j.rse.2018.08.005, 2018.  
662 Global Internal Displacement Monitoring Centre: Global Internal Displacement Database,  
663 [online] Available from: [https://www.internal-displacement.org/database/displacement-](https://www.internal-displacement.org/database/displacement-data)  
664 [data](https://www.internal-displacement.org/database/displacement-data), 2020.  
665 Goode, J. G., Yokelson, R. J., Susott, R. A. and Ward, D. E.: Trace gas emissions from  
666 laboratory biomass fires measured by open-path Fourier transform infrared spectroscopy:,  
667 *J. Chem. Inf. Model.*, 104(D17), 21237–21245, 1999.  
668 Hazell, P. and Wood, S.: Drivers of change in global agriculture., *Philos. Trans. R. Soc. Lond.*  
669 *B. Biol. Sci.*, 363(1491), 495–515, doi:10.1098/rstb.2007.2166, 2008.  
670 Hickman, Jonathan, E., Andela, N., Galy-Lacaux, C., Ossouhou, M., Dammers, E., Van Damme,  
671 M., Clarisse, L., Tsigaridis, K. and Bauer, S. E.: Continental and ecoregion-specific drivers of  
672 atmospheric NO<sub>2</sub> and NH<sub>3</sub> seasonality over Africa revealed by satellite observations,  
673 *Global Biogeochem. Cycles*, n.d.  
674 Hickman, J., Andela, N., Ossouhou, M., Galy-Lacaux, C., Tsigaridis, K. and Bauer, S.: Large  
675 reductions in NO<sub>2</sub> burden over north equatorial Africa from decline in biomass burning in  
676 spite of growing fossil fuel use, *Proc. Natl. Acad. Sci.*, n.d.  
677 Hickman, J. E., Dammers, E., Galy-Lacaux, C. and Van Der Werf, G. R.: Satellite evidence of  
678 substantial rain-induced soil emissions of ammonia across the Sahel, *Atmos. Chem. Phys.*,  
679 18(22), 16713–16727, doi:10.5194/acp-18-16713-2018, 2018.  
680 Huffman, G. J., Adler, R. F., Bolvin, D. T., Gu, G., Nelkin, E. J., Bowman, K. P., Hong, Y., Stocker,  
681 E. F. and Wolff, D. B.: The TRMM Multisatellite Precipitation Analysis (TMPA): Quasi-Global,  
682 Multiyear, Combined-Sensor Precipitation Estimates at Fine Scales, *J. Hydrometeorol.*, 8(1),  
683 38–55, doi:10.1175/jhm560.1, 2007.



684 Hurtmans, D., Coheur, P. F., Wespes, C., Clarisse, L., Scharf, O., Clerbaux, C., Hadji-Lazaro, J.,  
685 George, M. and Turquety, S.: FORLI radiative transfer and retrieval code for IASI, *J. Quant.*  
686 *Spectrosc. Radiat. Transf.*, 113(11), 1391–1408, doi:10.1016/j.jqsrt.2012.02.036, 2012.  
687 Idris, I.: *Livestock and conflict in South Sudan - K4D Helpdesk Report 484*, Brighton.  
688 [online] Available from:  
689 [https://assets.publishing.service.gov.uk/media/5c6abdec40f0b61a22792fd5/484\\_Livestock\\_and\\_Conflict\\_in\\_South\\_Sudan.pdf](https://assets.publishing.service.gov.uk/media/5c6abdec40f0b61a22792fd5/484_Livestock_and_Conflict_in_South_Sudan.pdf), 2018.  
690  
691 Kanter, D. R.: Nitrogen pollution: a key building block for addressing climate change, *Clim.*  
692 *Change*, 147(1–2), 11–21, doi:10.1007/s10584-017-2126-6, 2018.  
693 Kerzenmacher, T., Dils, B., Kumps, N., Blumenstock, T., Clerbaux, C., Coheur, P. F., Demoulin,  
694 P., García, O., George, M., Griffith, D. W. T., Hase, F., Hadji-Lazaro, J., Hurtmans, D., Jones, N.,  
695 Mahieu, E., Notholt, J., Paton-Walsh, C., Raffalski, U., Ridder, T., Schneider, M., Servais, C. and  
696 De Mazière, M.: Validation of IASI FORLI carbon monoxide retrievals using FTIR data from  
697 NDACC, *Atmos. Meas. Tech.*, 5(11), 2751–2761, doi:10.5194/amt-5-2751-2012, 2012.  
698 Korontzi, S., McCarty, J., Loboda, T., Kumar, S. and Justice, C.: Global distribution of  
699 agricultural fires in croplands from 3 years of Moderate Resolution Imaging  
700 Spectroradiometer (MODIS) data, *Global Biogeochem. Cycles*, 20(2), GB2021,  
701 doi:10.1029/2005GB002529, 2006.  
702 Krupa, S. V.: Effects of atmospheric ammonia (NH<sub>3</sub>) on terrestrial vegetation: A review,  
703 *Environ. Pollut.*, 124(2), 179–221, doi:10.1016/S0269-7491(02)00434-7, 2003.  
704 Lee, C., Martin, R. V., Van Donkelaar, A., Lee, H., Dickerson, R. R., Hains, J. C., Krotkov, N.,  
705 Richter, A., Vinnikov, K. and Schwab, J. J.: SO<sub>2</sub> emissions and lifetimes: Estimates from  
706 inverse modeling using in situ and global, space-based (SCIAMACHY and OMI)  
707 observations, *J. Geophys. Res. Atmos.*, 116(6), 1–13, doi:10.1029/2010JD014758, 2011.  
708 Lelieveld, J., Evans, J. S., Fnais, M., Giannadaki, D. and Pozzer, A.: The contribution of outdoor  
709 air pollution sources to premature mortality on a global scale, *Nature*, 525(7569), 367–371,  
710 doi:10.1038/nature15371, 2015.  
711 Nicholson, S., Some, B., McCollum, J., Nelkin, E., Klotter, D., Berte, Y., Diallo, B., Gaye, I.,  
712 Kpabeba, G., Ndiaye, O., Noukpozoukou, J., Tanu, M., Thiam, A., Toure, A. and Traore, A.:  
713 Validation of TRMM and other rainfall estimates with a high-density gauge dataset for West  
714 Africa. Part II: Validation of TRMM rainfall products, *J. Appl. Meteorol.*, 42, 1355–1368,



- 715 doi:Article, 2003.
- 716 Ossohou, M., Galy-Lacaux, C., Yoboué, V., Hickman, J. E., Gardrat, E., Adon, M., Darras, S.,  
717 Laouali, D., Akpo, A., Ouafou, M., Diop, B. and Opepa, C.: Trends and seasonal variability of  
718 atmospheric NO<sub>2</sub> and HNO<sub>3</sub> concentrations across three major African biomes inferred  
719 from long-term series of ground-based and satellite measurements, *Atmos. Environ.*, 207,  
720 148–166, 2019.
- 721 Pamela A. Matson, McDowell, W. H., Townsend, A. R. and Vitousek, P. M.: The globalization  
722 of N deposition: ecosystem consequences in tropical environments, *Biogeochemistry*, 46,  
723 67–83 [online] Available from: [http://academic.engr.arizona.edu/HWR/Brooks/GC572-](http://academic.engr.arizona.edu/HWR/Brooks/GC572-2004/readings/matson.pdf)  
724 [2004/readings/matson.pdf](http://academic.engr.arizona.edu/HWR/Brooks/GC572-2004/readings/matson.pdf), 1999.
- 725 Pommier, M., Law, K. S., Clerbaux, C., Turquety, S., Hurtmans, D., Hadji-Lazaro, J., Coheur, P.  
726 F., Schlager, H., Ancellet, G., Paris, J. D., Nédélec, P., Diskin, G. S., Podolske, J. R., Holloway, J. S.  
727 and Bernath, P.: IASI carbon monoxide validation over the Arctic during POLARCAT spring  
728 and summer campaigns, *Atmos. Chem. Phys.*, 10(21), 10655–10678, doi:10.5194/acp-10-  
729 10655-2010, 2010.
- 730 Pope, A., Burnett, R., Thun, M., EE, C., D, K., I, K. and GD, T.: Long-term Exposure to Fine  
731 Particulate Air Pollution, *J. Am. Med. Assoc.*, 287(9), 1132–1141,  
732 doi:10.1001/jama.287.9.1132, 2002.
- 733 Raleigh, C., Linke, A., Hegre, H. and Karlsen, J.: Introducing ACLED: An Armed Conflict  
734 Location and Event Dataset: Special Data Feature, *J. Peace Res.*, 47(5), 651–660,  
735 doi:<https://doi.org/10.1177/0022343310378914>, 2010.
- 736 Robinson, T. P., Wint, G. R. W., Conchedda, G., Van Boeckel, T. P., Ercoli, V., Palamara, E.,  
737 Cinardi, G., D'Aietti, L., Hay, S. I. and Gilbert, M.: Mapping the Global Distribution of  
738 Livestock, *PLoS One*, 9(5), e96084, doi:10.1371/journal.pone.0096084, 2014.
- 739 Roteta, E., Bastarrika, A., Padilla, M., Storm, T. and Chuvieco, E.: Development of a Sentinel-2  
740 burned area algorithm: Generation of a small fire database for sub-Saharan Africa, *Remote*  
741 *Sens. Environ.*, 222(November 2018), 1–17, doi:10.1016/j.rse.2018.12.011, 2019.
- 742 Rufino, M. C., Rowe, E. C., Delve, R. J. and Giller, K. E.: Nitrogen cycling efficiencies through  
743 resource-poor African crop-livestock systems, *Agric. Ecosyst. Environ.*, 112(4), 261–282,  
744 doi:10.1016/j.agee.2005.08.028, 2006.
- 745 Sauvage, B., Gheusi, F., Thouret, V., Cammas, J. P., Duron, J., Escobar, J., Mari, C., Mascart, P.



746 and Pont, V.: Medium-range mid-tropospheric transport of ozone and precursors over  
747 Africa: Two numerical case studies in dry and wet seasons, *Atmos. Chem. Phys.*, 7(20),  
748 5357–5370, doi:10.5194/acp-7-5357-2007, 2007.

749 Stevens, C. J., David, T. I. and Storkey, J.: Atmospheric nitrogen deposition in terrestrial  
750 ecosystems: Its impact on plant communities and consequences across trophic levels,  
751 *Funct. Ecol.*, 32(7), 1757–1769, doi:10.1111/1365-2435.13063, 2018.

752 Sutton, M. A., Reis, S., Riddick, S. N., Dragosits, U., Nemitz, E., Theobald, M. R., Tang, Y. S.,  
753 Braban, C. F., Vieno, M., Dore, A. J., Mitchell, R. F., Wanless, S., Daunt, F., Fowler, D., Blackall,  
754 T. D., Milford, C., Flechard, C. R., Loubet, B., Massad, R., Cellier, P., Personne, E., Coheur, P. F.,  
755 Clarisse, L., Van Damme, M., Ngadi, Y., Clerbaux, C., Skøth, C. A., Geels, C., Hertel, O., Wichink  
756 Kruit, R. J., Pinder, R. W., Bash, J. O., Walker, J. T., Simpson, D., Horváth, L., Misselbrook, T. H.,  
757 Bleeker, A., Dentener, F. and de Vries, W.: Towards a climate-dependent paradigm of  
758 ammonia emission and deposition, *Philos. Trans. R. Soc. B Biol. Sci.*, 368(1621), 20130166–  
759 20130166, doi:10.1098/rstb.2013.0166, 2013.

760 Tian, D. and Niu, S.: A global analysis of soil acidification caused by nitrogen addition,  
761 *Environ. Res. Lett.*, 10(2), 024019, doi:10.1088/1748-9326/10/2/024019, 2015.

762 USDA Agricultural Air Quality Task Force: Ammonia Emissions : What To Know Before You  
763 Regulate, Washington, DC. [online] Available from:  
764 <http://www.nrcs.usda.gov/wps/portal/nrcs/detail/national/air/taskforce/?cid=stelprdb1>  
765 268645, 2014.

766 Vitousek, P., Naylor, R., Crews, T., David, M., Drinkwater, L., Holland, E., Johnes, P.,  
767 Katzenberger, J., Martinelli, L. A., Matson, P. A., Nziguheba, G., Ojima, D., Palm, C. A.,  
768 Robertson, G., Sanchez, P., Townsend, A. and Zhang, F.: Nutrient Imbalances in Agricultural  
769 Development, *Science* (80-. ), 324, 1519–1520, 2009.

770 Di Vittorio, C. A. and Georgakakos, A. P.: Land cover classification and wetland inundation  
771 mapping using MODIS, *Remote Sens. Environ.*, 204(May 2017), 1–17,  
772 doi:10.1016/j.rse.2017.11.001, 2018.

773 Vrieling, A., de Beurs, K. M. and Brown, M. E.: Variability of African farming systems from  
774 phenological analysis of NDVI time series, *Clim. Change*, 109(3–4), 455–477,  
775 doi:10.1007/s10584-011-0049-1, 2011.

776 De Wachter, E., Barret, B., Le Flochmoën, E., Pavelin, E., Matricardi, M., Clerbaux, C., Hadji-



777 Lazaro, J., George, M., Hurtmans, D., Coheur, P. F., Nedelec, P. and Cammas, J. P.: Retrieval of  
778 MetOp-A/IASI CO profiles and validation with MOZAIC data, *Atmos. Meas. Tech.*, 5(11),  
779 2843–2857, doi:10.5194/amt-5-2843-2012, 2012.

780 Warner, J. X., Dickerson, R. R., Wei, Z., Strow, L. L., Wang, Y. and Liang, Q.: Increased  
781 atmospheric ammonia over the world’s major agricultural areas detected from space,  
782 *Geophys. Res. Lett.*, 44(6), 2875–2884, doi:10.1002/2016GL072305, 2017.

783 Whitburn, S., Van Damme, M., Kaiser, J. W., Van Der Werf, G. R., Turquety, S., Hurtmans, D.,  
784 Clarisse, L., Clerbaux, C. and Coheur, P. F.: Ammonia emissions in tropical biomass burning  
785 regions: Comparison between satellite-derived emissions and bottom-up fire inventories,  
786 *Atmos. Environ.*, 121, 42–54, doi:10.1016/j.atmosenv.2015.03.015, 2015.

787 World Bank: World Bank Open Data, World Bank Open Data [online] Available from:  
788 <https://www.data.worldbank.org> (Accessed 2 February 2019), n.d.

789 Yegbemey, R. N., Kabir, H., Awoye, O. H. R., Yabi, J. A. and Paraíso, A. A.: Managing the  
790 agricultural calendar as coping mechanism to climate variability: A case study of maize  
791 farming in northern Benin, West Africa, *Clim. Risk Manag.*, 3, 13–23,  
792 doi:10.1016/j.crm.2014.04.001, 2014.

793 Yokelson, R. J., Christian, T. J., Karl, T. G. and Guenther, A.: The tropical forest and fire  
794 emissions experiment: laboratory fire measurements and synthesis of campaign, *Rev. Int.*  
795 *Acupunt.*, 8, 3509–3527, doi:10.1016/s1887-8369(09)71579-0, 2008.

796 Zheng, B., Chevallier, F., Ciais, P., Yin, Y. and Wang, Y.: On the Role of the Flaming to  
797 Smoldering Transition in the Seasonal Cycle of African Fire Emissions, *Geophys. Res. Lett.*,  
798 45(21), 11,998–12,007, doi:10.1029/2018GL079092, 2018.

799